PHYSICAL REVIEW D **89,** 014505 (2014)

Proton decay matrix elements on the lattice

Y. Aoki,[1,2,*] E. Shintani,[2,†] A. Soni[3,‡]
(RBC and UKQCD Collaborations)

[1]*Kobayashi-Maskawa Institute for the Origin of Particles and the Universe (KMI), Nagoya University, Nagoya 464-8602, Japan*
[2]*RIKEN-BNL Research Center, Brookhaven National Laboratory, Upton, New York 11973, USA*
[3]*High Energy Theory Group, Brookhaven National Laboratory, Upton, New York 11973, USA*
(Received 1 May 2013; published 13 January 2014)

Hadronic matrix elements of proton decays are essential ingredients for bridging the grand unification theory to low-energy observables like the proton lifetime. In this paper we nonperturbatively calculate the matrix elements, relevant for the process of a nucleon decaying into a pseudoscalar meson and an antilepton through generic baryon-number-violating four-fermi operators. Lattice QCD with $2+1$ flavor dynamical domain-wall fermions with the *direct* method—which is the direct measurement of the matrix elements from the three-point function without using chiral perturbation theory—is used for this study in order to have good control over the errors due to lattice discretization effects, operator renormalization, and chiral extrapolation. The relevant form factors for possible transition processes from an initial proton or neutron to a final pion or kaon induced by all types of three-quark operators are obtained through three-point functions of the (nucleon)-(three-quark operator)-(meson) with physical kinematics. In this study all the relevant systematic uncertainties of the form factors are taken into account for the first time, and the total error is found to be in the range 30%–40% for the π and 20%–40% for the K final states.

DOI: 10.1103/PhysRevD.89.014505 PACS numbers: 11.15.Ha, 12.10.Dm, 12.38.Gc

I. INTRODUCTION

Proton decay is a "smoking gun" of physics beyond the standard model and is a natural outcome of grand unified theories (GUTs) [1,2]. The process occurs through baryon-number-changing interactions mediated by the heavy new particles. Dominant modes are X and Y gauge-boson exchanges for GUTs and color-triplet Higgs multiplets for supersymmetric (SUSY) GUTs [3,4]. Recent Super-Kamiokande experiments have reported bounds on the proton partial lifetime, such as $\tau > 8.2 \times 10^{33}$ years for the $p \to e^+\pi^0$ channel [5,6]—which is typical for gauge-boson exchange—or $\tau > 2.3 \times 10^{33}$ years for $p \to K^+\bar{\nu}$ [7] and $\tau > 1.6 \times 10^{33}$ years for $p \to K^0\bar{\mu}^+$ [8], both of which are favored for some SUSY GUTs. There have been many arguments for a constraint on the proton lifetime from various types of GUT models (for a comprehensive review see Ref. [9] and references therein). In order to constrain the parameter space in GUT models with a reliable bound, the removal of all the theoretical uncertainties is highly desirable. One of the important elements—which can be made less uncertain using current knowledge—is the hadronic contribution to proton decay matrix elements. Lattice QCD calculations can lead to reducing the uncertainties in the hadronic matrix element of a nucleon decaying into a pseudoscalar meson, and thus they can provide relevant information for the proton lifetime bound and help experimental plans for the future [10].

The estimates for proton decay matrix elements in lattice QCD have been significantly improved by removing systematic errors, one by one, since the first attempts in the 1980s [11–13]. A decade ago the JLQCD Collaboration [14] performed an extensive calculation of proton decay matrix elements using the Wilson fermion action and an operator renormalization estimated by one-loop lattice perturbation theory in the quenched approximation with both the "direct" method, which is a direct measurement of matrix elements from three-point functions, and the "indirect" method, which is an effective estimate through low-energy constants in tree-level chiral perturbation theory, calculated with two-point functions. A few years later the JLQCD and CP-PACS joint collaboration carried out a continuum extrapolation of the low-energy constants for the indirect method [15] to control the uncertainty of the large discretization error. Using the direct method, the RBC collaboration [16] performed the analysis with quenched domain-wall fermions (DWFs) and nonperturbative renormalization, where—thanks to the almost exact chiral symmetry of the DWFs—the discretization error of $O(a)$ was essentially removed and the error in the renormalization factor associated with the use of lattice perturbation theory was also eliminated. The RBC Collaboration also performed the DWF calculation using the indirect method with the quenched approximation as

*yaoki@kmi.nagoya-u.ac.jp
†shintani@riken.jp
‡adlersoni@gmail.com

well as by unquenching the u and d quarks [16], and later the RBC and UKQCD Collaborations extended the DWF calculation with the indirect method using three dynamical quarks (u, d and s) [17]. In this way, one of the uncontrolled systematic uncertainties coming from the quenched approximation was removed.

A striking (but perhaps not surprising) outcome of the comparison of the results from the direct and indirect calculations—though so far only performed with the quenched approximation—is that the indirect method could overestimate the matrix elements by a factor of about 2 [16]. To fully control the systematic uncertainties, therefore, one needs to perform the direct calculation with the $N_f = 2 + 1$ dynamical simulations and a nonperturbative operator renormalization.

In this paper we provide the nonperturbative estimate of the proton decay matrix elements using the direct method with the dynamical $N_f = 2 + 1$ (degenerate u, d and physical s quarks) flavor lattice QCD with DWFs. The DWF ensemble for $N_f = 2 + 1$ at the lattice cutoff $a^{-1} \sim 1.7\,\mathrm{GeV}$ with 300–700 MeV pion masses [18] in the RBC/UKQCD Collaboration is used for this purpose, which enables us to evaluate hadronic matrix elements including almost all systematic errors on the lattice.

This paper is organized as follows. In Sec. II we explain the definition and properties of the matrix elements as well as their relation to the proton partial decay width. The method of extraction for the matrix elements from three-point functions on the lattice is expressed in Sec. III, and in Sec. IV we present our setup and a detailed analysis to obtain the matrix elements and evaluate their systematic uncertainties. Section V is devoted to a summary and outlook.

II. PROTON DECAY MATRIX ELEMENTS

A. Effective Lagrangian and matrix elements

Baryon-number-violating operators appearing in the leading low-energy effective Hamiltonian are constructed by the possible combinations of dimension-six (three quarks and one lepton) operators as SU(3) color singlets and $\mathrm{SU}_L(2) \times U_Y(1)$ invariants. Following the notation of Refs. [19–21], the four-fermi operators are expressed as

$$O^{(1)}_{abcd} = (D^i_a, U^j_b)_R (q^{k\alpha}_c, l^\beta_d)_L \varepsilon^{ijk} \varepsilon^{\alpha\beta}, \tag{1}$$

$$O^{(2)}_{abcd} = (q^{i\alpha}_a, q^{j\beta}_b)_L (U^k_c, l_d)_R \varepsilon^{ijk} \varepsilon^{\alpha\beta}, \tag{2}$$

$$\tilde{O}^{(4)}_{abcd} = (q^{i\alpha}_a, q^{j\beta}_b)_L (q^{k\gamma}_c, l^\delta_d)_L \varepsilon^{ijk} \varepsilon^{\alpha\delta} \varepsilon^{\beta\gamma}, \tag{3}$$

$$O^{(5)}_{abcd} = (U^i_a, D^j_b)_R (U^k_c, l_d)_R \varepsilon^{ijk}, \tag{4}$$

with the generic lepton field l, and where the quark field of the left-handed part is q and those of the right-handed part are U and D (i.e., up and down types). The indices a, b, c, d denote the generation number of the fermion, i, j, k denote the color SU(3) indices, and α, β, γ, δ are SU(2) indices. The inner product is defined as $(x, y)_{R/L} = x^T C P_{R/L} y$, which has a charge conjugation matrix C and a chiral projection $P_{R/L}$. The baryon number violation (which still preserves the B–L number) in GUT models is generally expressed as a low-energy effective Hamiltonian with the above dimension-six operators. The leading term of the effective Hamiltonian at low energies is represented as

$$\mathcal{L}B = \sum_I C^I [(qq)(ql)]^I + \cdots = -\sum_I C^I [\bar{l}^c \mathcal{O}_{qqq}]^I + \cdots, \tag{5}$$

where $C^I = C^I(\mu)$ is the Wilson coefficient with renormalization scale μ of the operator $[(qq)(ql)]^I$, with q being a light quark flavor (u, d, or s). The operator is one of those appearing in Eqs. (1–4) and is renormalized at μ. All the details of the (SUSY) GUT are captured in the coefficients $C^I(\mu)$. The ellipsis indicates the higher-order operators, which are suppressed by the inverse power of the heavy mass scale. The index I distinguishes the type of operator with respect to the quark-lepton flavor and chirality. The three-quark operator reads

$$\mathcal{O}^{\Gamma\Gamma'}_{qqq} = (qq)_\Gamma q_{\Gamma'} = \varepsilon^{ijk} (q^{iT} C P_\Gamma q^j) P_{\Gamma'} q^k, \tag{6}$$

where the color singlet contraction is taken. Dirac spinor indices are omitted in the above equation. In the following we may denote the three-quark operators as $\mathcal{O}^{\Gamma\Gamma'}$. Γ and Γ' denote the chirality, either R or L, and the bracket denotes the contractions among the Dirac spinors.

We calculate the transition matrix elements of the dimension-six operators with an initial nucleon (proton or neutron, $N = p$, n) state and a final state containing a pseudoscalar meson [$P = (\pi, K, \eta)$] and an antilepton ($\bar{l}$),

$$\langle P(\vec{p}), l(\vec{q}, s) | [\vec{l}^c \mathcal{O}^{\Gamma\Gamma'}] | N(\vec{k}) \rangle = \bar{v}^c_l(q, s) \langle P(\vec{p}) | \mathcal{O}^{\Gamma\Gamma'} | N(\vec{k}, s) \rangle, \tag{7}$$

where the three-dimensional momenta are $\vec{p}$ for the final pseudoscalar, $\vec{k}$ for the initial nucleon, and $\vec{q} = \vec{p} - \vec{k}$ for the final lepton, which is determined from momentum conservation. Neglecting the electroweak interaction of the lepton, the amplitude $\langle l(\vec{q}, s) | \bar{l}^c | 0 \rangle = \bar{v}^c_l(\vec{q}, s)$ of the lepton part can be captured in the wave function of the on-shell lepton state at momentum $\vec{q}$ for the spin-s component. The matrix element $\langle P(\vec{p}) | \mathcal{O}^{\Gamma\Gamma'} | N(\vec{k}, s) \rangle$ is parametrized by the relevant form factor $W_0(q^2)$ and the irrelevant one $W_1(q^2)$ as

$$\langle P(\vec{p}) | \mathcal{O}^{\Gamma\Gamma'} | N(\vec{k}, s) \rangle = P_{\Gamma'} \left[W_0^{\Gamma\Gamma'}(q^2) - \frac{i\not{q}}{m_N} W_1^{\Gamma\Gamma'}(q^2) \right] u_N(k, s). \tag{8}$$

W_0 and W_1 are defined for each matrix element with the three-quark operator renormalized in the minimal-subtraction scheme ($\bar{M}S$) with the naïve-dimensional-regularization (NDR) at the scale μ and are functions of the square of the four-momentum transfer $q = k - p$. Using the on-shell condition, the total matrix element as shown in Eq. (7) is given by

$$\begin{aligned}
&\bar{\nu}_l^c(q,s)\langle P(\vec{p})|\mathcal{O}^{\Gamma\Gamma'}|N(\vec{k},s)\rangle \\
&\quad = \bar{\nu}_l^c(q,s)P_{\Gamma'}\left[W_0^{\Gamma\Gamma'}(q^2) - \frac{i\not{q}}{m_N}W_1^{\Gamma\Gamma'}(q^2)\right]u_N(k,s) \\
&\quad = \bar{\nu}_l^c(\vec{q},s)P_{\Gamma'}u_N(\vec{k},s)W_0^{\Gamma\Gamma'}(0) + O(m_l/m_N), \qquad (9)
\end{aligned}$$

with $i\not{q}v_l = m_l v_l$ and $W_1 \simeq W_0$ [16]. Since $-q^2 = m_l^2$ is much smaller than the nucleon mass squared in the case of $l = e$, ν, we set $q^2 = 0$ and ignore the second term in Eq. (9). Taking only the relevant form factor will be a good approximation even for $l = \mu$, as $m_\mu/m_N \sim 10\%$, which is smaller than the total error of W_0 in this study.

Once the relevant form factor W_0 is obtained in lattice QCD, the partial decay width of the decay $N \to P + \bar{l}$ is given by

$$\Gamma(N \to P + \bar{l}) = \frac{m_N}{32\pi}\left[1 - \left(\frac{m_P}{m_N}\right)^2\right]^2\left|\sum_I C^I W_0^I(N \to P)\right|^2 \qquad (10)$$

with the perturbative estimate of the Wilson coefficient C^I in the GUT models [9]. Note that multiplying C^I and W_0^I cancels their renormalization-scale dependence.

The different chirality combinations of the matrix elements are related through the parity transformation as

$$\langle P;\vec{p}|\mathcal{O}^{RL}|N;\vec{k},s\rangle = \gamma_0\langle P;-\vec{p}|\mathcal{O}^{LR}|N;-\vec{k},s\rangle, \qquad (11)$$

$$\langle P;\vec{p}|\mathcal{O}^{LL}|N;\vec{k},s\rangle = \gamma_0\langle P;-\vec{p}|\mathcal{O}^{RR}|N;-\vec{k},s\rangle, \qquad (12)$$

which indicates that the four chirality combinations $(\Gamma\Gamma') = (RL)$, (LL), (LR), (RR) are reduced to two different combinations, $(\Gamma\Gamma') = (RL), (LL)$. In the following Γ' is fixed in a left-handed chirality, and the short-hand notation $W_{0,1}^{\Gamma L} \equiv W_{0,1}^{\Gamma}$ is used. Under an exchange symmetry between u and d, there are the following relations between the proton and neutron matrix elements:

$$\langle\pi^0|(ud)_\Gamma u_L|p\rangle = \langle\pi^0|(du)_\Gamma d_L|n\rangle, \qquad (13)$$

$$\langle\pi^+|(ud)_\Gamma d_L|p\rangle = -\langle\pi^-|(du)_\Gamma u_L|n\rangle, \qquad (14)$$

$$\langle K^0|(us)_\Gamma u_L|p\rangle = -\langle K^+|(ds)_\Gamma d_L|n\rangle, \qquad (15)$$

$$\langle K^+|(us)_\Gamma d_L|p\rangle = -\langle K^0|(ds)_\Gamma u_L|n\rangle, \qquad (16)$$

$$\langle K^+|(ud)_\Gamma s_L|p\rangle = -\langle K^0|(du)_\Gamma s_L|n\rangle, \qquad (17)$$

$$\langle K^+|(ds)_\Gamma u_L|p\rangle = -\langle K^0|(us)_\Gamma d_L|n\rangle, \qquad (18)$$

$$\langle\eta|(ud)_\Gamma u_L|p\rangle = -\langle\eta|(du)_\Gamma d_L|n\rangle. \qquad (19)$$

A negative sign comes from the interpolation operator of the proton or neutral pion by the exchange of u and d. Furthermore, in the SU(2) isospin limit there is an additional relation between Eq. (13) and Eq. (14),

$$\langle\pi^0|(ud)_\Gamma u_L|p\rangle = \sqrt{2}\langle\pi^+|(ud)_\Gamma d_L|p\rangle. \qquad (20)$$

Therefore there are twelve principal matrix elements, which we will calculate in this paper.

III. CALCULATION SCHEME FOR THE FORM FACTORS

To obtain the matrix element we make use of the ratio of the three-point function of the (proton)-($O^{\Gamma L}$)-(meson) and the two-point function of the nucleon and meson. Such a ratio is represented as

$$R_3(t,t_1,t_0;\vec{p},P) = \frac{\sum_{\vec{x},\vec{x}_1} e^{i\vec{p}(\vec{x}_1-\vec{x})}\mathrm{tr}[P\langle 0|J_P^{\mathrm{gs}}(\vec{x}_1,t_1)\mathcal{O}^{\Gamma L}(\vec{x},t)\bar{J}_p^{\mathrm{gs}}(\vec{0},t_0)|0\rangle]}{\sum_{\vec{x},\vec{x}_1} e^{i\vec{p}(\vec{x}_1-\vec{x})}\langle 0|J_P^{\mathrm{gs}}(\vec{x}_1,t_1)J_P^{\mathrm{gs}\dagger}(\vec{x},t)|0\rangle\sum_{\vec{x}}\mathrm{tr}[P_4\langle 0|J_p^{\mathrm{gs}}(\vec{x},t)\bar{J}_p^{\mathrm{gs}}(\vec{0},t_0)|0\rangle]}\sqrt{Z_P^{\mathrm{gs}}(\vec{p})Z_p^{\mathrm{gs}}}L_\sigma^3, \qquad (21)$$

where J_P^{gs} and J_p^{gs} are the interpolating fields for the pseudoscalar and proton, respectively. These interpolating operators are made of quark fields smeared using the gauge-invariant Gaussian smearing [22] with the parameters optimized separately for the meson and the proton. In the periodic lattice the injected spatial momentum is $\vec{p} = 2\pi\vec{n}/L_\sigma$, where $\vec{n}$ is an integer vector $0 \le n_i \le L_\sigma - 1$, and L_σ is the spatial extension of the lattice. "tr" represents a trace over spinor indices, and $\mathcal{P}$ is a spin projection matrix. The three-point function in the numerator is constructed using the quark propagator with the sequential source method at the pseudoscalar sink location.

$Z_{P,p}$ indicates the amplitude of the overlap of the interpolating field to the on-shell state,

TABLE I. Lattice parameters, the estimate of the hadron masses, and the squared momentum transfer from the initial-state nucleon to the final-state meson for each parameter set are shown. The lines with a blank $m_s^{\rm val}$ entry show the kinematic parameters for the pion final state and the nucleon mass, while those with a $m_s^{\rm val}$ entry are for the kaon final states. The two $-q^2$ values in each line are for the two different momenta injected to the meson, $\vec{p}^2 = (\pi/12)^2, 2(\pi/12)^2$, respectively, where the $-q^2$ is shown in units of GeV using $a^{-1} = 1.73(3)$ GeV [18]. The fitting range used for the mass estimates are $6 \le t \le 23$ for the pion and kaon and $5 \le t \le 13$ for the nucleon.

$(m_{ud}^{\rm sea}, m_s^{\rm sea})$	$m_{ud}^{\rm val}$	$m_s^{\rm val}$	m_π	m_K	m_N	$-q^2$(GeV^2)		# configs.	# meas.
(0.005,0.04)	0.005		0.1897(5)		0.656(16)	−0.129	0.241	202	404
	0.005	0.0343		0.3131(5)		0.017	0.325		
	0.005	0.04		0.3322(5)		0.039	0.337		
(0.01,0.04)	0.01		0.2420(6)		0.705(16)	−0.162	0.194	150	150
	0.01	0.0343		0.3328(6)		−0.035	0.280		
	0.01	0.04		0.3510(6)		−0.011	0.295		
(0.02,0.04)	0.02		0.3228(6)		0.790(10)	−0.218	0.137	100	100
	0.02	0.0343		0.3681(6)		−0.142	0.189		
	0.02	0.04		0.3849(6)		−0.114	0.208		
(0.03,0.04)	0.03		0.3880(7)		0.912(11)	−0.391	−0.020	90	90
	0.03	0.0343		0.4003(6)		−0.364	−0.000		
	0.03	0.04		0.4160(6)		−0.330	0.025		

$$\langle P(\vec{p})|J_P^{\rm gs\dagger}(0)|0\rangle = \sqrt{Z_P^{\rm gs}(\vec{p})}, \tag{22}$$

$$\langle 0|J_p^{\rm gs}(0)|p(\vec{0}, s)\rangle = \sqrt{Z_p^{\rm gs}}u_p(k,s), \tag{23}$$

with the proton Dirac spinor normalized as $\bar{u}_p(k,s)\times u_p(k,s') = 2m_N\delta_{ss'}$. In this study we always take the proton to be at rest. Note that the operator of the nucleon interpolating field is not uniquely determined, and we make use of the two possible proton operators,

$$J_p = \varepsilon^{ijk}(u^{iT}C\gamma_5 d^j)u^k, \qquad \varepsilon^{ijk}(u^{iT}C\gamma_4\gamma_5 d^j)u^k. \tag{24}$$

A numerical comparison of the above two types of nucleon interpolating operators will be shown in the next section.

In the simulation we take the sufficiently large separation between t_0 and t_1 in Eq. (21), so we have a range of t where the three- and two-point functions in the ratio are dominated by the ground states. Then the ratio leads to its asymptotic form,

$$\lim_{t_1-t,t-t_0\to\infty} R_3(t,t_1,t_0;\vec{p},P) = R_3^{\rm asym}(\vec{p},P) = {\rm tr}\left[PP_L\left(W_0^\Gamma(q^2) - \frac{i\not{q}}{m_N}W_1^\Gamma(q^2)\right)\right], \tag{25}$$

where q^2 is the squared momentum transfer from the initial proton to the final pseudoscalar meson state $q^2 = (k-p)^2$. We employ two different projection matrices, $P = P_4$ or $iP_4\gamma_j$, where we use $P_4 = (1+\gamma_4)/2$ to subtract the contribution from the parity partner of the proton and to disentangle W_0 and W_1. By solving the linear equations

$$R_3^{\rm asym}(p,P_4) = W_0^\Gamma(q^2) - \frac{iq_4}{m_N}W_1^\Gamma(q^2), \tag{26}$$

$$R_3^{\rm asym}(p,iP_4\gamma_j) = \frac{q_j}{m_N}W_1^\Gamma(q^2), \tag{27}$$

the relevant form factor W_0 can be obtained.

IV. NUMERICAL CALCULATION OF THE PROTON DECAY FORM FACTORS

A. Lattice setup

We use the gauge configurations generated for $2+1$ flavor dynamical domain-wall fermions with the Iwasaki gauge action developed by the RBC and UKQCD collaborations [18]. The lattice volume is $24^3 \times 64$ and the size of the fifth dimension is $L_s = 16$. The gauge coupling

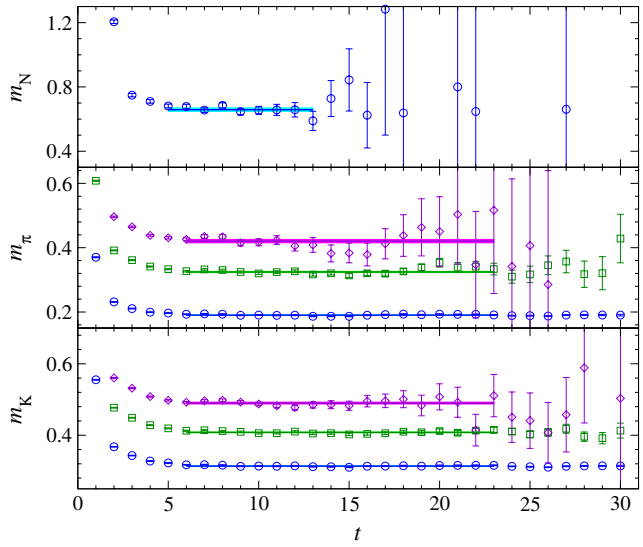

FIG. 1 (color online). Effective mass plot of the nucleon (top), pion (middle), and kaon (bottom) at momentum squared $n_p^2 = 0$ (circle), $n_p^2 = 1$ (square), and $n_p^2 = 2$ (diamond), which correspond to $p = (0,0,0)$, $(\pi/12,0,0)$, and $(\pi/12,\pi/12,0)$, respectively. For the nucleon we use a gauge-invariant Gaussian source/sink, and for the meson we use a (Kuramashi-)wall source and a -invariant Gaussian sink. This is for the lightest quark masses $m_{ud} = 0.005$ and $m_s = 0.0343$. The solid line (colored band) indicates the central value (statistical error) obtained by fitting.

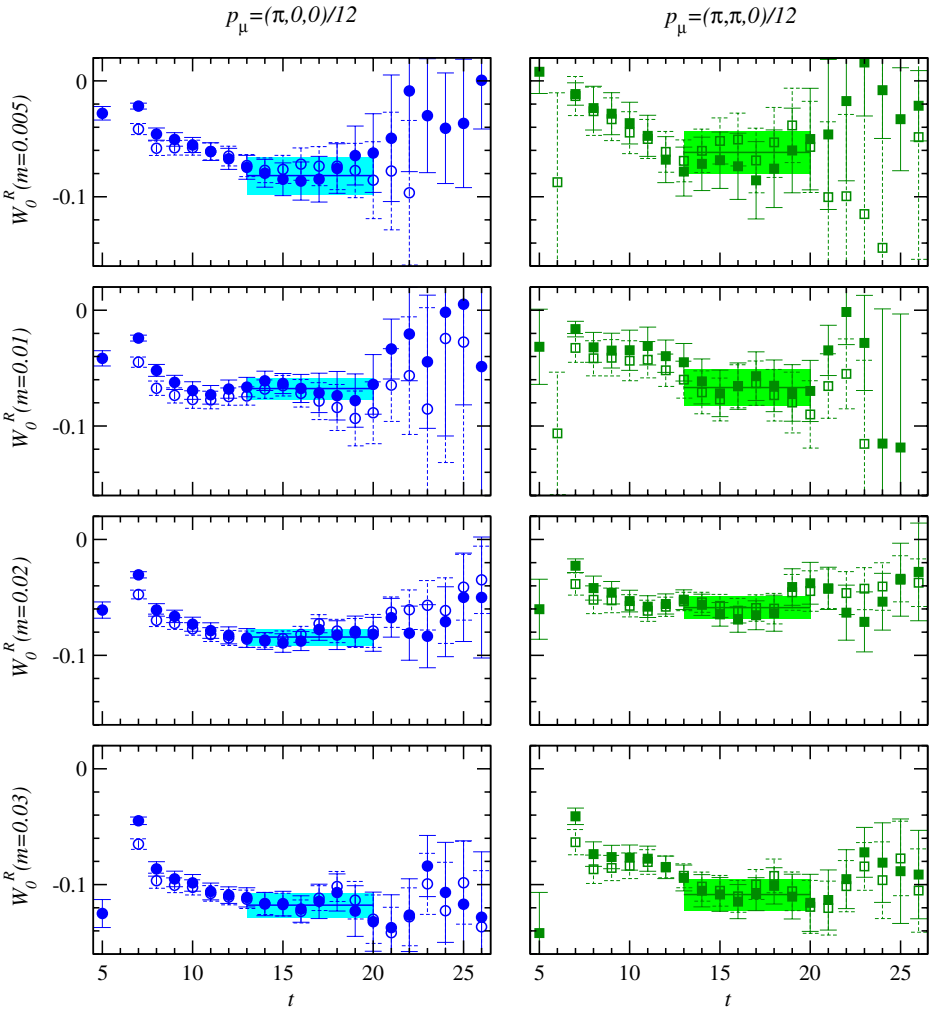

FIG. 2 (color online). W_0^R for the $p \to \pi^0$ decay channel is plotted as a function of operator time [t in Eq. (21)]. The proton source is located at $t = 5$, and the π^0 sink is at $t = 27$. Different symbols show the two different proton interpolating fields, which correspond to $(u^T C\gamma_5 d)u$ (open) and $(u^T C\gamma_4\gamma_5 d)u$ (filled). The horizontal solid line indicates the central value of the constant fit to both plateaus in the range $13 \le t \le 20$ simultaneously. The shaded area indicates the one-sigma error band.

$\beta = 2.13$ corresponds to $a^{-1} = 1.73(3)$ GeV. This is the same ensemble as the in previous indirect method study [17]. The boundary condition is periodic for the gauge field, and it is spatially periodic and temporally antiperiodic for the fermion fields. We use four different unitary u, d quark masses for chiral extrapolation, and one unitary and one partially quenched strange-quark mass for the study of the strange-quark mass dependence of the final $K^{0,+}$ kaon state. For later convenience let us introduce the quark mass $\tilde{m}$, which includes the additive renormalization due to the inexact chiral symmetry of the domain-wall fermions at a finite extent of the fifth dimension. We define

$$\tilde{m} = m + m_{\mathrm{res}} \tag{28}$$

as the multiplicatively renormalizable mass with m in the lattice action, where the residual mass m_{res} for the lattice used in this study has been calculated as $m_{\mathrm{res}} = 0.003152(43)$ [18]. The form factors of the nucleon-to-pion matrix elements depend on $\tilde{m}_{ud}$ for the degenerate u- and d-quark mass and the squared momentum transfer q^2. For the nucleon-to-kaon matrix elements, the strange-quark mass $\tilde{m}_s$ enters as an additional parameter.

In the computation of the two-point and three-point functions on the lattice, we employ a gauge-invariant Gaussian smearing with the optimized parameter $(n_G, \sigma) = (40, 5.0)$ for the baryon source/sink and $(n_G, \sigma) = (16, 3.0)$ for the meson sink, where the APE-smeared gauge links with $(N, c) = (12, 0.4)$ are as defined in Ref. [23]. The time slices for the nucleon source t_0 and meson sink t_1 are set as $(t_0, t_1) = (5, 37)$ or (27,59). The baryon-number-violating operator at time t moves between them ($t_0 < t < t_1$). We use the first and second smallest but nonzero momenta $p = (\pi/12, 0, 0)$, $(\pi/12, \pi/12, 0)$ on the periodic lattice for the meson. The statistics used for each ensemble are summarized in Table I, as well as the valence masses used

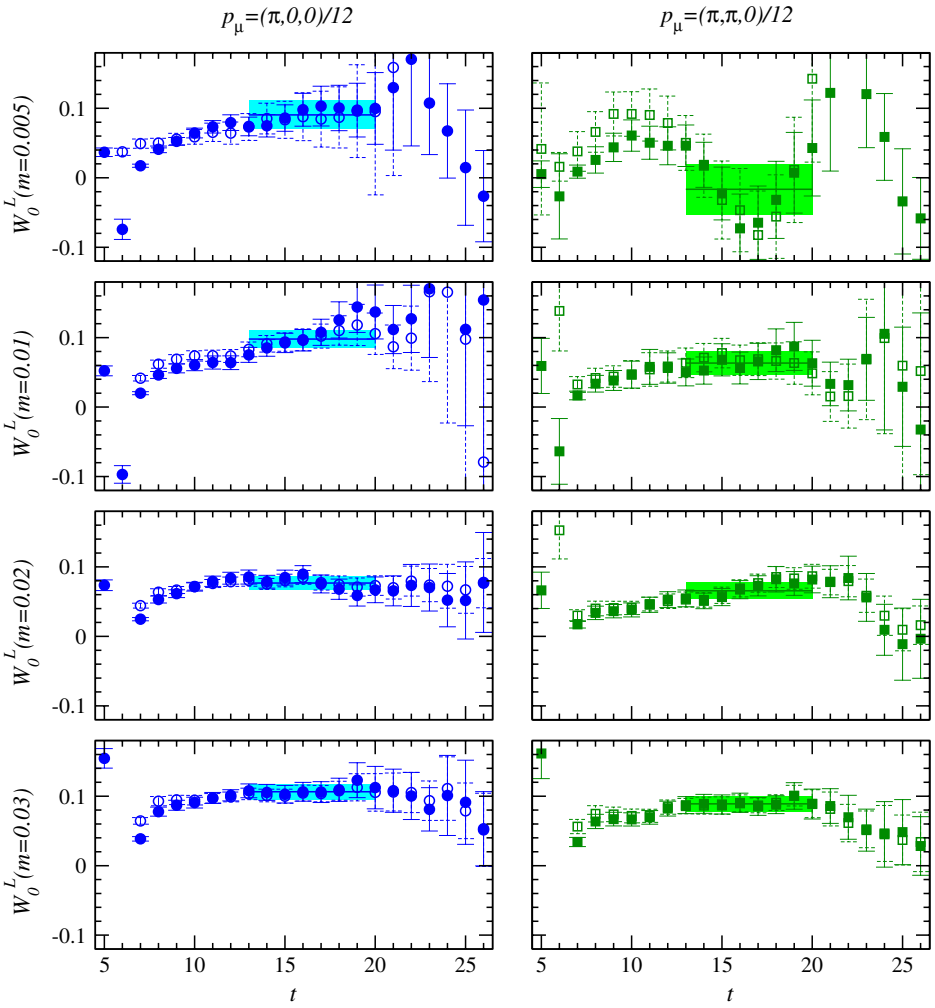

FIG. 3 (color online). W_0^L for the $p \to \pi^0$ decay channel is plotted as a function of operator time. The symbols are same as in Fig. 2.

and the measured q^2. Measurements are done with each of the 40 hybrid Monte Carlo (HMC) trajectories for the ensembles with $m_{ud} = 0.005$ and 0.01, or with each of the 20 HMC trajectories for $m_{ud} = 0.02$ and 0.03. We alternate the source time slice between $t_0 = 5$ and $t_0 = 27$ from one configuration to the next for $m_{ud} = 0.01$, 0.02 and 0.03, while we measure both $t_0 = 5$ and 27 for all configurations at $m_{ud} = 0.005$. (Therefore the number of measurements is double the number of configurations.)

The multiplicative renormalization factors that convert the lattice three-quark operators in Eqs. (13–15) into those in the $\bar{M}S$ NDR scheme have been calculated through the regularization-invariant momentum-subtraction nonperturbative renormalization procedure [17] as

$$U(\mu = 2\ \mathrm{GeV})_{LL} = 0.662(10)(53), \tag{29}$$

$$U(\mu = 2\ \mathrm{GeV})_{RL} = 0.665(8)(53). \tag{30}$$

The first error is statistical and the second is systematic. (A systematic error of 8% was estimated in Ref. [17] as a truncation effect of the perturbative expansion.)

In Fig. 1 we show the effective mass of the nucleon, pion, and kaon two-point functions which enter in the denominator of Eq. (21). The effective mass at time t is constructed with data at t and $t+1$, and we can observe the plateau region whose starting point is $t = 5$ for the nucleon and $t = 6$ for the pseudoscalar. Therefore, the denominator of Eq. (21) is dominated by the ground states for t satisfying both $t - t_0 \geq 5$ and $t_1 - t \leq 6$.

B. Measurement of the form factor and kinematics

Figures 2 and 3 show the form factor W_0 of the $p \to \pi^0$ channel in Eqs. (26) and (27) as a function of the time position t of the three-quark operator. The open and filled symbols correspond to results in two different nucleon interpolating operators, $(q^T C\gamma_5 q)q$ and $(q^T C\gamma_4\gamma_5 q)q$, respectively. To obtain the value of W_0, a simultaneous fit of these two effective W_0's is performed at the plateau in the range $13 \leq t \leq 20$, where the two W_0's appear to be consistent and the contamination from the excited states dies out. The same range is used for all the parameters and all

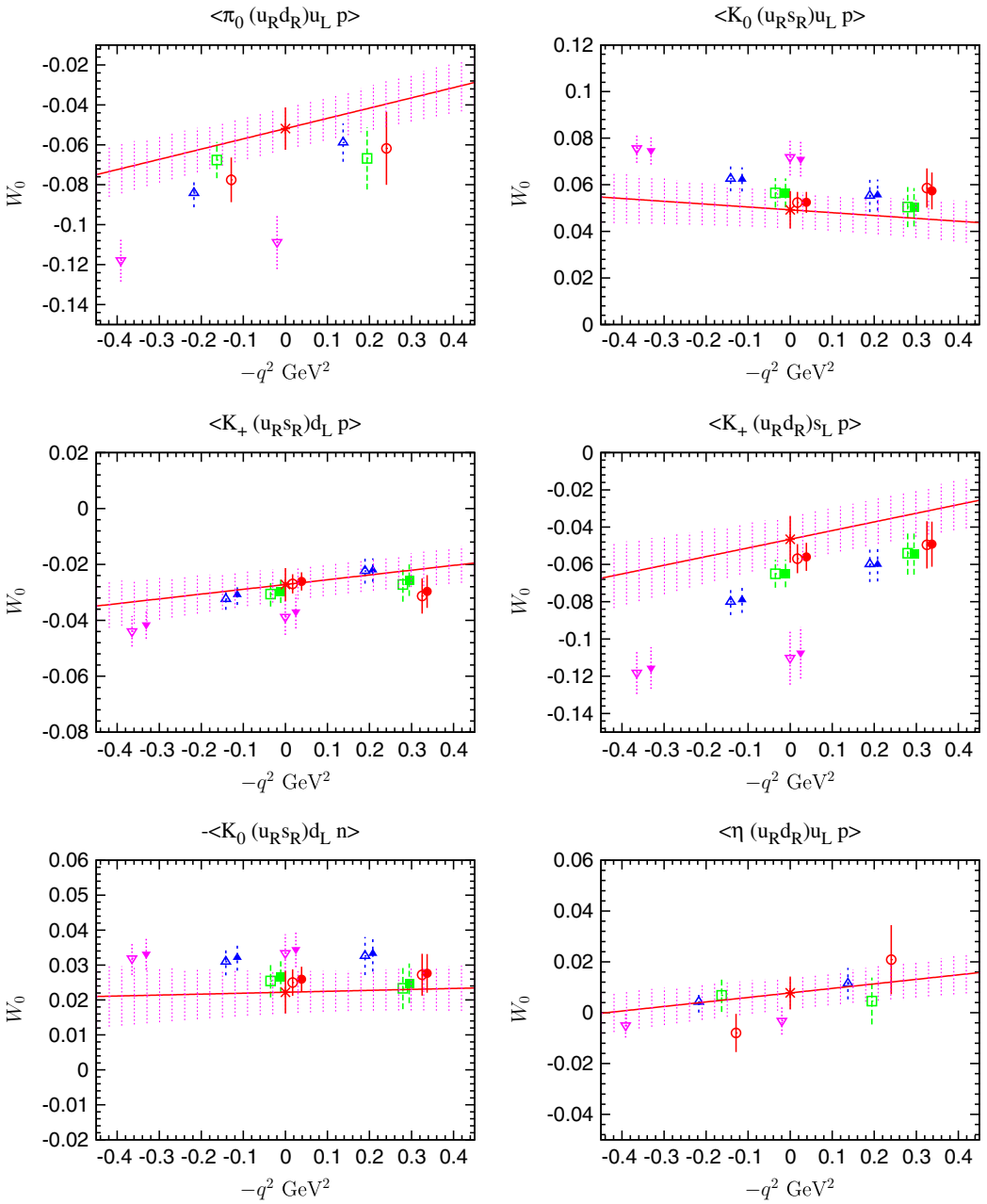

FIG. 4 (color online). q^2 dependence of $W_0^R(q^2)$ at all quark masses in lattice units. We plot the results at $m_{ud} = 0.005$ (circle), $m_{ud} = 0.01$ (square), $m_{ud} = 0.02$ (up-triangle), and $m_{ud} = 0.03$ (down-triangle). In the figure for $K^{0,+}$, the results at $m_s = 0.0343$ and $m_s = 0.04$ are represented by the open and closed symbols, respectively. The solid lines (bands) show the global fit function (and its error) after taking the extrapolation into the physical quark mass using all of the points. The star symbol is the result at the physical kinematics using the global fit.

the matrix elements. Figures 4 and 5 show $W_0^{R/L}$ for each channel as a function of q^2.

The form factors in the physical kinematics are calculated from the extrapolation or interpolation with the momentum and quark masses. For the physical kinematics of proton decay into a meson and lepton final state, $-q^2$ is equivalent to the lepton mass squared in the relevant form factor $W_0(q^2)$. In the lattice computation, however, the quark masses are additional parameters that need to be tuned toward the physical pion and kaon masses. Therefore we have three parameters to tune: the degenerate u-, d-quark mass $\tilde{m}_{ud}$, the strange-quark mass $\tilde{m}_s$, and the meson momentum $|\vec{p}|$. In our simulation, the $\tilde{m}_{ud} \to \tilde{m}_{ud}^{\rm phys}$ limit is taken by an extrapolation and the $\tilde{m}_s \to \tilde{m}_s^{\rm phys}$ limit is taken by an interpolation, where the physical quark mass in lattice units is realized by the limit

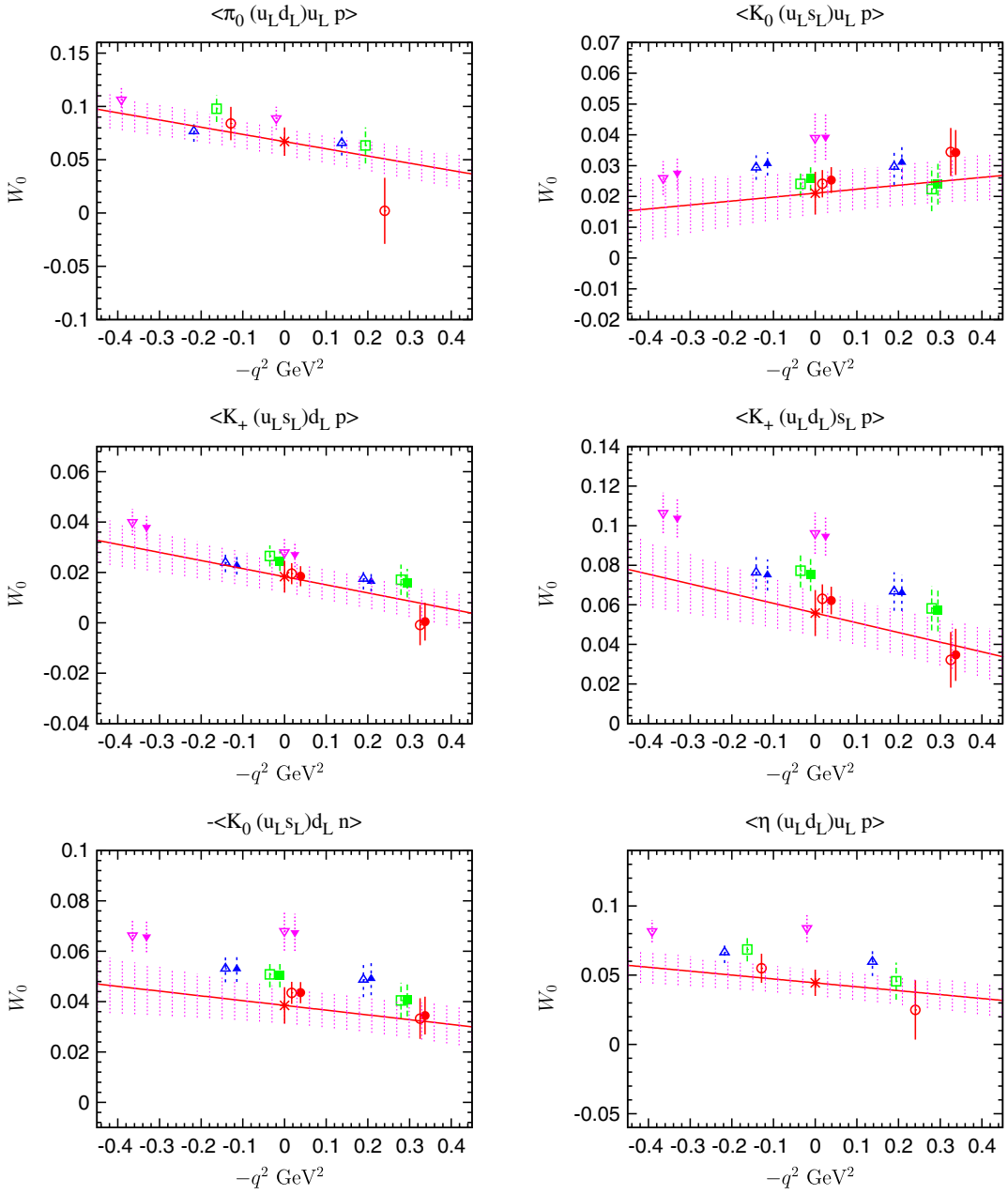

FIG. 5 (color online). q^2 dependence of $W_0^L(q^2)$ at all quark masses. Symbols are the same as in Fig. 4.

$$\tilde{m}_{ud}^{\text{phys}} = 0.001385, \tag{31}$$

$$\tilde{m}_{s}^{\text{phys}} = 0.03785, \tag{32}$$

where the values reproduce the experimental hadron mass ratios, m_π/m_Ω and m_K/m_Ω, and the pion and kaon masses over the mass of Ω^- [18].

We employ two different procedures for taking the above limit. One is a global fit with a function that depends on both the quark mass and q^2, and thus W_0 at the physical point is straightforwardly obtained. The other procedure is to sequentially take two limits: first we take $q^2 \to 0$, and then we take the quark mass to the physical point. In this procedure W_0 at the physical point is obtained with the second limit. In the next section we will show numerical results obtained using these procedures.

C. Extrapolation to physical kinematics with global fitting

In the global fitting, to obtain the form factor in the physical kinematics we use the ansatz of the linear function,

$$F_{W_0}^{\pi,\eta}(\tilde{m}_{ud}, q^2) = A_0 + A_1\tilde{m}_{ud} + A_2 q^2, \tag{33}$$

TABLE II. Table of results for the renormalized $W_0^{R/L}(\mu = 2\ \mathrm{GeV})$ in GeV^2 after global and sequential fitting. The error is only statistical. For the global fitting, we show the results with three different fitting mass ranges, which are all in the range $0.005 \le m_{ud} \le 0.03$ (r_{full}), excluding the heaviest mass $m_{ud} = 0.03$ (r_{light}) and the lightest mass $m_{ud} = 0.005$ (r_{heavy}). For the sequential fitting, we show the results including all the masses.

	Global				Sequential	
Matrix element	r_{full}	χ^2/d.o.f.	r_{light}	r_{heavy}	r_{full}	χ^2/d.o.f.
$\langle\pi^0\vert(ud)_R u_L\vert p\rangle$	−0.103(23)	1.4	−0.132(29)	−0.072(34)	−0.114(22)	2.2
$\langle\pi^0\vert(ud)_L u_L\vert p\rangle$	0.133(29)	1.4	0.156(41)	0.142(38)	0.123(28)	1.1
$\langle K^0\vert(us)_R u_L\vert p\rangle$	0.098(15)	0.4	0.103(19)	0.092(29)	0.093(15)	0.1
$\langle K^0\vert(us)_L u_L\vert p\rangle$	0.042(13)	0.4	0.044(16)	0.037(20)	0.037(14)	0.1
$\langle K^+\vert(us)_R d_L\vert p\rangle$	−0.054(11)	0.8	−0.060(13)	−0.052(21)	−0.049(13)	0.6
$\langle K^+\vert(us)_L d_L\vert p\rangle$	0.036(12)	0.8	0.040(15)	0.041(18)	0.041(12)	0.6
$\langle K^+\vert(ud)_R s_L\vert p\rangle$	−0.093(24)	0.6	−0.108(28)	−0.082(39)	−0.088(25)	0.9
$\langle K^+\vert(ud)_L s_L\vert p\rangle$	0.111(22)	0.6	0.121(28)	0.115(37)	0.117(23)	0.7
$\langle K^+\vert(ds)_R u_L\vert p\rangle$	−0.044(12)	0.1	−0.043(14)	−0.041(20)	−0.044(12)	0.1
$\langle K^+\vert(ds)_L u_L\vert p\rangle$	−0.076(14)	0.3	−0.082(17)	−0.076(24)	−0.078(14)	0.5
$\langle\eta\vert(ud)_R u_L\vert p\rangle$	0.015(14)	1.3	−0.002(19)	0.031(19)	0.017(14)	1.2
$\langle\eta\vert(ud)_L u_L\vert p\rangle$	0.088(21)	0.7	0.094(29)	0.094(28)	0.076(21)	0.4

$$F^K_{W_0}(\tilde{m}_{ud}, \tilde{m}_s, q^2) = B_0 + B_1\tilde{m}_{ud} + B_2\tilde{m}_s + B_3 q^2, \quad (34)$$

with the free parameters A_i and B_i. $F^{\pi,\eta}_{W_0}$ is used for the pion or η final state and $F^K_{W_0}$ is used for the kaon final state. This procedure is the same as that employed in the previous study [16]. We use four different quark masses, two different strange-quark masses, and the two lowest nonzero spacial momenta, and therefore the total number of data points is eight for π and η or sixteen for the kaon final states. The results obtained with the global fit using all the data are shown in the second column in Table II. It turns out that the simple linear function as described in Eqs. (33) and (34) is in good agreement with the lattice data for all channels, which is indicated by the reasonable χ^2/d.o.f. (≤ 1.4). The fit results $F^{\pi,\eta}_{W_0}(\tilde{m}^{\mathrm{phys}}_{ud}, q^2)$, $F^K_{W_0}(\tilde{m}^{\mathrm{phys}}_{ud}, \tilde{m}^{\mathrm{phys}}_s, q^2)$ as a function of q^2 at the physical masses are shown in Figs. 4 and 5.

D. Extrapolation to physical kinematics with sequential fitting

In this procedure we first take the linear extrapolation or interpolation to $q^2 = 0$ with two spatial momentum points in each mass $\tilde{m}$ and then take a chiral extrapolation to the physical quark mass. Figures 6 and 7 plot the results at the $q^2 = 0$ point as a function of $\tilde{m}_{ud}$ after taking the $q^2 = 0$ limit. In the chiral extrapolation of the fitted data at $q^2 = 0$ we adopt the linear function as

$$f^{\pi,\eta}_{W_0}(\tilde{m}_{ud}) = a_0 + a_1\tilde{m}_{ud}, \quad (35)$$

$$f^K_{W_0}(\tilde{m}_{ud}, \tilde{m}_s) = b_0 + b_1\tilde{m}_{ud} + b_2\tilde{m}_s \quad (36)$$

for the pion, η final state or the kaon final state, respectively. Here a_i and b_i are the free fitting parameters. From Figs. 6 and 7 we observe that the linear function describes the lattice results quite well for each matrix element with four different mass points, except that the data for the pion and eta in Fig. 6 seems to be less consistent with the linear ansatz. The difference between the four-point fit and the three-point fit will be used in the estimate of the systematic error discussed later. The results are shown in Table II (see the column marked as "Sequential").

E. Systematic errors

The systematic errors due to using the extrapolation (or interpolation) into physical kinematics ($q^2 = 0$ limit), and the contributions of the finite-volume effect and nonzero lattice spacing will be discussed in this section. This work uses the lattice scale estimated in Ref. [18] and the renormalization constant shown in Eqs. (29) and (30). To estimate the total error separately from the statistical error, the systematic errors in the extrapolation, the finite-size effect, and the lattice artifact—together with the error of the lattice scale and that of the nonperturbative renormalization procedure—are all added in quadrature.

At the target mass and momentum point $(\tilde{m}_{ud}, \tilde{m}_s, q^2) = (\tilde{m}^{\mathrm{phys}}_{ud}, \tilde{m}^{\mathrm{phys}}_s, 0)$, no chiral singularity is expected. Therefore, if the simulations are made closer to the target, the linear approximation to the fitting function becomes arbitrarily precise. However, as the simulated points might not be close enough to assume linearity, we need to assess the systematic error due to the choice of this approximation. This systematic error is regarded as an effect of higher order than $O(\tilde{m}_{ud})$ and $O(q^2)$. Note that the higher-order effect beyond $O(\tilde{m}_s)$ is safely neglected as its variation around the physical point is very small, as can be estimated by comparing the results with $m_s = 0.0343$ and 0.04 in Figs. 4 and 5.

The main results of the relevant form factors are employed similarly as those by the global fit with $0.005 \le m_{ud} \le 0.03$ (see the second column of Table II). Note that r denotes the different fitting ranges,

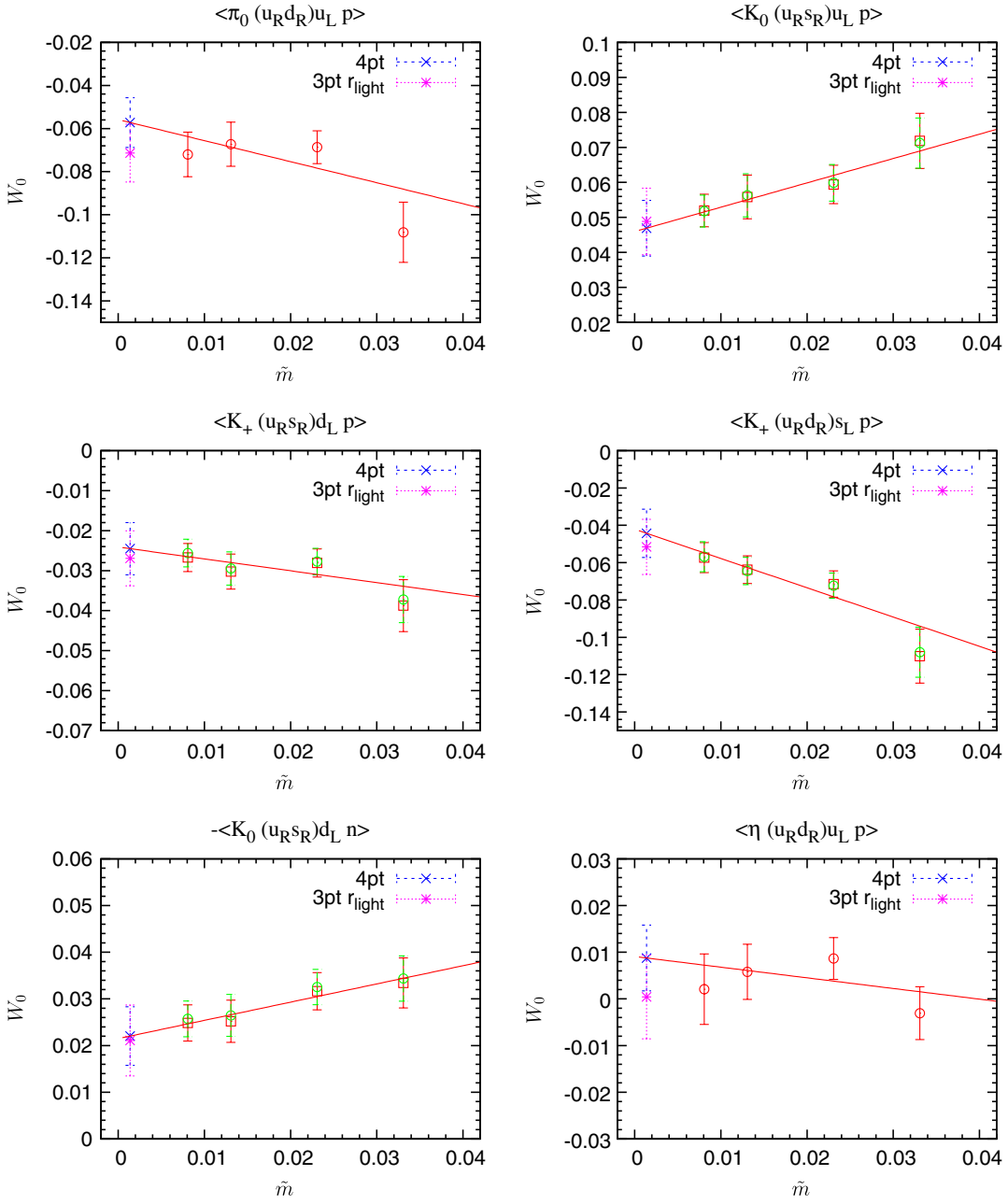

FIG. 6 (color online). Results of $W_0^R(0)$ at different $\tilde{m} = m_{ud} + m_{\rm res}$. The different open symbols shown in the matrix element of the kaon final state are the results at different values of the partially quenched strange-quark mass, $m_s = 0.0343$ (circle) and $m_s = 0.04$ (square). Straight lines show the linearly fit function with all four quark masses. For the matrix element of $p \to K$, these are the results after taking the physical strange-quark mass. The cross symbol is the result at the physical light and strange masses with four fitting points, and the star symbol is with three fitting points using the range of $r_{\rm light}$ defined in the text. We discuss the systematic uncertainties by using the discrepancy between the different fitting points (for example, four fitting points and three fitting points) in Section IV E.

$$r_{\rm full}: [0.005, 0.03], \quad r_{\rm heavy}: [0.01, 0.03], \quad r_{\rm light}: [0.005, 0.02], \tag{37}$$

which are also used in Table II. The variations of the results caused by removing the largest and smallest $\tilde{m}_{ud}$ from the global fit, together with the difference between the result in the sequential fit and the main result, provide the systematic errors coming from the uncertainty of the fitting function for the extrapolation to the physical kinematics and the finite-size effect (FSE).

The uncertainty in the extrapolation due to a higher-order effect than linearity in the quark mass (and also q^2) is estimated by the variance between the results in $r_{\rm full}$ and those in $r_{\rm light}$ and the variance between the results with the global

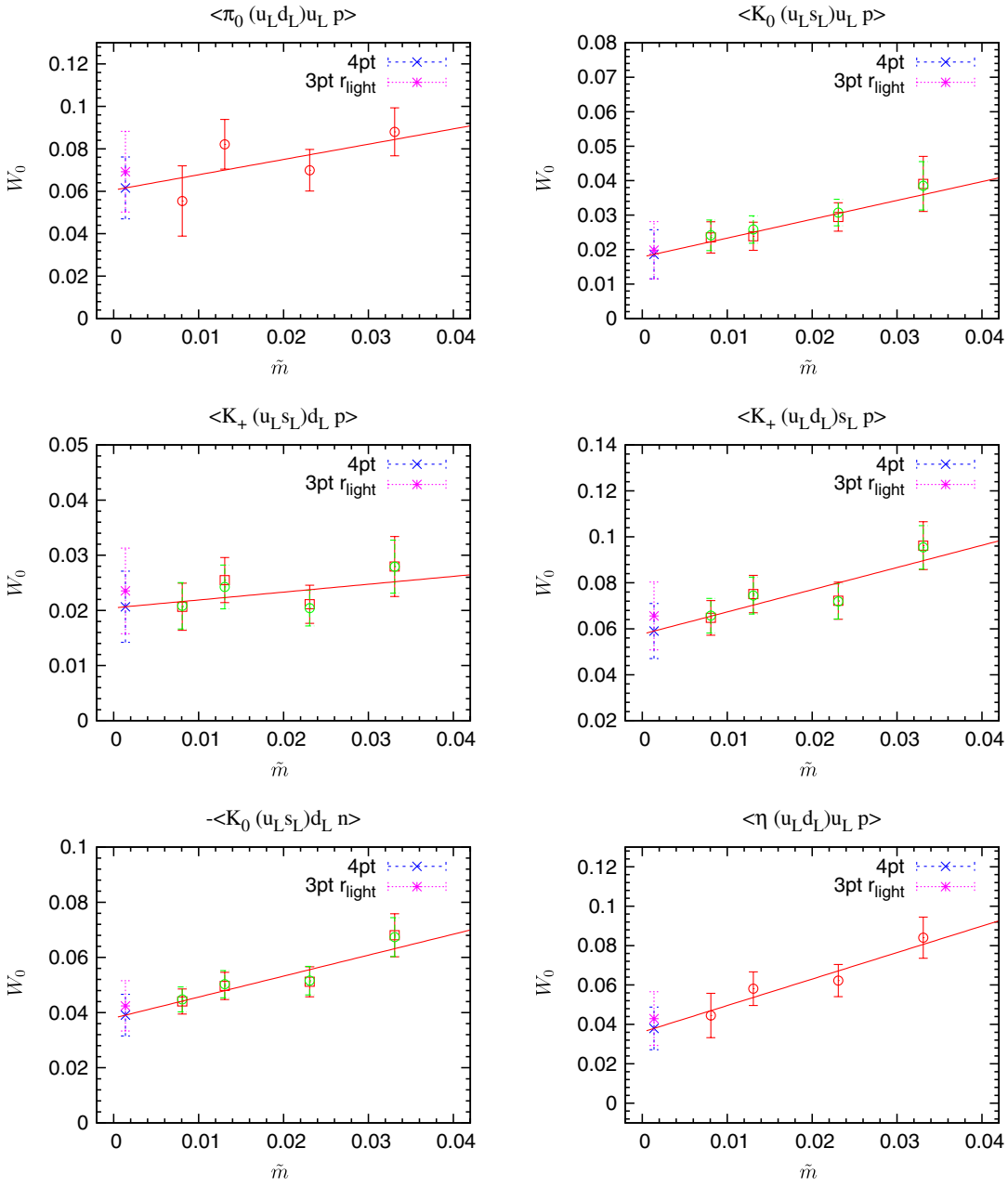

FIG. 7 (color online). Results of $W_0^L(0)$ with the same symbols as in Fig. 6.

fit and those with the sequential fit. By comparing the region with and without the heavy mass $m = 0.03$, which is close to the physical strange-quark mass, we estimate the $O(\tilde{m}^2)$ effect. Furthermore, since the sequential fitting procedure (explained in the previous subsection) takes into account the mass dependence of the q^2 slope, we estimate the systematic error of the extrapolation to the physical kinematics as a part of the higher-order effect [e.g., $\mathcal{O}(\tilde{m}q^2)$ terms] beyond the $\tilde{m}$ and q^2 linear approximation by comparing with the results in the global fit.

On the other hand, the difference between results the in r_{full} and r_{heavy} is expected to probe at least a part of the FSE since the lightest point is affected the most by the FSE rather than the $O(\tilde{m}^2)$ effect. Such an estimate of the FSE was used in the calculation of the nucleon axial charge g_A [24,25], in which a significant FSE was observed in the lightest quark mass in the same gauge ensemble. [This is also suggested by the fact that the relevant form factor W_0 for a pion final state is proportional to $(1 + g_A)$ in the leading order of baryon chiral perturbation theory; see Ref. [16].] Therefore neglecting data at the lightest mass $m = 0.005$ in the fitting region might result in less contamination from the FSE (see also Fig. 10 of Ref. [25]).

TABLE III. Final results of the renormalized $W_0^{L/R}(\mu = 2\ \mathrm{GeV})$ for individual matrix elements and the error budget of the statistical and systematic uncertainties. The first and second errors in $W_0^{L/R}$ represent the statistical and systematic errors, respectively. The third column denotes the total error, which is estimated by adding the statistical and systematical errors in quadrature. The fourth column, denoted as χ, shows the systematic error of the mass and momentum extrapolation/interpolation estimated by the variance of the extrapolation to physical kinematics, and the fifth column shows the uncertainties from lattice artifacts (as explained in the text). The last two columns show the uncertainties of the renormalization factor (ΔZ) and lattice spacing (Δa^{-1}). We also show the $p \to \pi^+\nu$ decay matrix element using the SU(2) isospin relation in Eq. (20).

Matrix element	$W_0(\mu = 2\ \mathrm{GeV})\mathrm{GeV}^2$		Total error (%)	Systematic error budget χ	$\mathcal{O}(a^2)$	ΔZ	Δa^{-1}
$\langle\pi^0\|(ud)_R u_L\|p\rangle$	−0.103	(23) (34)	40	0.033	0.005	0.008	0.004
$\langle\pi^0\|(ud)_L u_L\|p\rangle$	0.133	(29) (28)	30	0.026	0.007	0.011	0.005
$\langle\pi^+\|(ud)_R d_L\|p\rangle$	−0.146	(33) (48)	40	0.047	0.007	0.011	0.006
$\langle\pi^+\|(ud)_L d_L\|p\rangle$	0.188	(41) (40)	30	0.037	0.010	0.016	0.007
$\langle K^0\|(us)_R u_L\|p\rangle$	0.098	(15) (12)	20	0.007	0.005	0.008	0.003
$\langle K^0\|(us)_L u_L\|p\rangle$	0.042	(13) (8)	36	0.007	0.002	0.003	0.001
$\langle K^+\|(us)_R d_L\|p\rangle$	−0.054	(11) (9)	26	0.008	0.003	0.004	0.002
$\langle K^+\|(us)_L d_L\|p\rangle$	0.036	(12) (7)	39	0.007	0.002	0.003	0.001
$\langle K^+\|(ud)_R s_L\|p\rangle$	−0.093	(24) (18)	32	0.016	0.005	0.008	0.003
$\langle K^+\|(ud)_L s_L\|p\rangle$	0.111	(22) (16)	25	0.012	0.006	0.009	0.004
$\langle K^+\|(ds)_R u_L\|p\rangle$	−0.044	(12) (5)	30	0.003	0.002	0.004	0.002
$\langle K^+\|(ds)_L u_L\|p\rangle$	−0.076	(14) (9)	22	0.006	0.004	0.006	0.003
$\langle\eta\|(ud)_R u_L\|p\rangle$	0.015	(14) (17)	147	0.017	0.001	0.001	0.001
$\langle\eta\|(ud)_L u_L\|p\rangle$	0.088	(21) (16)	30	0.014	0.004	0.007	0.003

The systematic error including both the higher-order effect [$O(\tilde{m}^2)$, $O((q^2)^2)$, $O(\tilde{m}q^2)$] and the FSE is evaluated by adding in quadrature the difference between the global and sequential fitting results in the range of r_{full} and the maximum difference between the global fitting results in the range of (r_{full}, r_{light}) and (r_{full}, r_{heavy}), even though this procedure may be too conservative. The magnitude is shown in the column denoted as "Extrapolation" in Table III.

The discretization error of $O(a)$ may arise from the inexact chiral symmetry due to a finite L_s. However, as the size of the chiral symmetry breaking is small after the additive mass shift [Eq. (27)] is performed, $m_{\mathrm{res}}a \simeq 3 \times 10^{-3}$, this effect can be safely neglected. Here the dominant discretization error at $O(a^2)$ has been estimated using the scaling study of a hadronic observable performed with this and finer lattice ensembles [18]. The observed discrepancy in the spectroscopy of the light meson (Fig. 26 in Ref. [18]) with the two lattice spacings is up to 1%–2%, which amounts to a roughly 5% discretization error of the form factor W_0 assuming the $O(a^2)$ scaling. We take this 5% as the $O(a^2)$ error,

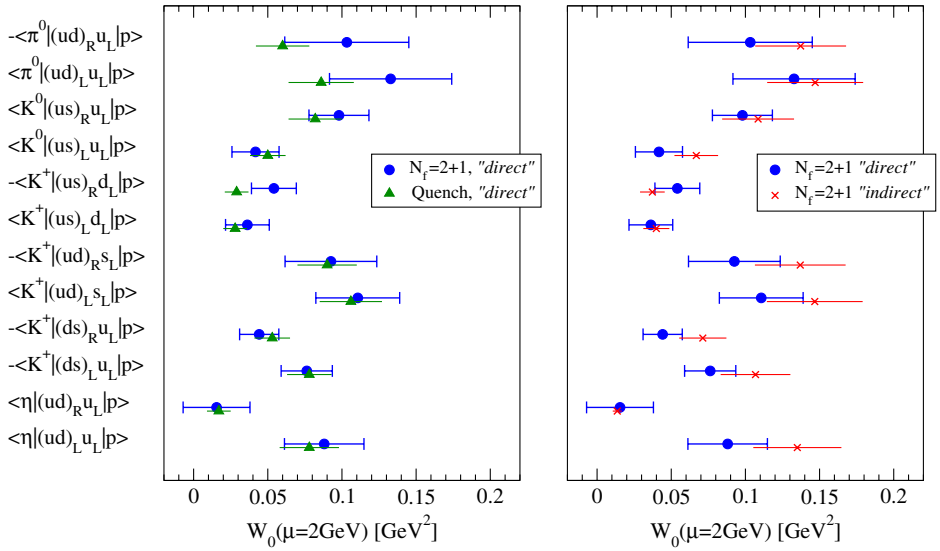

FIG. 8 (color online). Summary of $W_0^{L/R}(\mu = 2\ \mathrm{GeV})$ for twelve principal matrix elements. Filled circles show the present results, and for comparison the results in quenched QCD (triangles) and the indirect method using chiral perturbation theory (crosses) are plotted as well.

which is more conservative than a naive power counting $(a\Lambda_{\rm QCD})^2 \sim 0.02$, with $\Lambda_{\rm QCD} = 250$ MeV.

We also take into account the error coming from the uncertainty of the lattice spacing, which is given as $a^{-1} = 1.73(3)$ GeV, and the error of the renormalization constant, which is given in Eq. (29) or Eq. (30).

We ignore the partially quenched effect of the strange quark—which is due to the small mismatch of the sea and valence strange masses—for the matrix element of the K^+, K^0 meson final state. Since the valence strange-quark mass dependence of W_0 is negligibly small—as shown in Figs. 6 and 7—this effect is also negligible. Note that we also do not consider the effect of disconnected diagrams in the matrix elements of the η in the final state, but we note that the result is valid assuming a flavor SU(3) degenerate valence quark $m_{ud}^{\rm val} = m_s^{\rm val}$ and ignoring the partially quenched effect of the strange quark.

F. Results of proton decay matrix elements

Table III summarizes the results of the relevant form factor $W_0(q^2)$ of proton decay for all the principal matrix elements [Eqs. (13), (15–19)] at $q^2 = 0$. The central values are those obtained with the global fit on q^2 and the simulated quark masses for the physical kinematics $\tilde{m}_{ud} \to \tilde{m}_{ud}^{\rm phys}$, $\tilde{m}_s \to \tilde{m}_s^{\rm phys}$, and $q^2 \to 0$, with the $r_{\rm full}$ range for m_{ud}. The values in the first parenthesis are the statistical errors. The budget of the systematic error is shown in the last four columns. These four errors are added in quadrature to give the total systematic error shown in the second parenthesis for each value of the form factors.

Figure 8 shows the results of the form factors with the error bars expressing the total error when the statistical and systematic errors are added in quadrature, which are marked as "$N_f = 2 + 1$." The two panels compare the results with the old ones using some approximation. The left panel compares the results with the quenched approximation in the direct method [16]. The right panel shows those results obtained with the indirect method in the same ensembles [17]. The sizable error for "$N_f = 2 + 1$" in the current analysis prevents us from seeing any significant difference from the quenched or indirect results. For phenomenological applications, however, one should clearly use our $N_f = 2 + 1$ results with the direct method with the total error instead of the previous results [16,17], because each previous approximation has used systematic uncertainties that were not even estimated.

V. SUMMARY AND OUTLOOK

We have presented the lattice calculation of proton decay matrix elements using $2 + 1$ flavor dynamical domain-wall fermions, which are essential ingredients to estimate the nucleon lifetime in grand unified theories. The direct method using the three-point function of the (nucleon)-(operator)-(meson) with nonperturbative renormalization was applied on a volume $L_\sigma^3 \simeq 3$ fm^3. Previous calculations had undermined the estimate of the systematic uncertainties on the matrix elements at the physical kinematics. This work made it possible to control these uncertainties for the first time by removing most of them, while the remaining uncertainties were given with their estimates. The uncertainties that have been eliminated here are those due to the quenched approximation [16] and the use [17] of the indirect method with tree-level baryon chiral perturbation theory. The estimated uncertainties are the error in the extrapolation in the quark mass and meson momentum, the finite-volume effect, the discretization error, the error in the nonperturbative renormalization, and the uncertainty of the lattice scale. The relevant form factors $W_0(q^2 = 0)$ of the twelve principal matrix elements [Eqs. (13), (15–19)]—from which one can calculate those for the entire nucleon-to-pseudoscalar-meson process—have been evaluated and summarized in Table III with their error estimates.

Although we have established an estimate of the proton decay matrix element with all the errors, the total errors are fairly large (30%–40% for the π final state and 20%–40% for the K final state). One of the major uncertainties is the statistical error, especially for the $p \to e^+\pi^0$ decay mode, which could have influenced the size of the error of the combined chiral extrapolation and the finite-volume effect. A significant improvement of the current results is expected with the adoption of the newly developed technique for the reduction of the statistical error [26], which will be addressed in future work. However, we want to emphasize that for now one should use the results in this paper with the stated total errors in any serious phenomenological application.

ACKNOWLEDGMENT

We thank the members of the RBC/UKQCD collaborations for their valuable help with comments and encouragement. We especially would like to thank Peter Boyle, Paul Cooney, Chris Dawson, Luigi Del Debbio, Taku Izubuchi, Chulwoo Jung, Adam Lichtle, Chris Maynard, and Robert Tweedie. Numerical calculations were performed on QCDOC computers of the USQCD Collaboration and the RIKEN BNL Research Center, for which we thank the US DOE and RIKEN BNL Research Center. A. S. is supported by U.S. DOE Contract No. DE-AC02-98CH10886. This work is also supported, in part, by JSPS Kakenhi Grant Nos. 21540289, 22224003 (Y. A.), and by MEXT Kakenhi Grant No. 23105714 (E. S.).

[1] J. C. Pati and A. Salam, Phys. Rev. Lett. **31**, 661 (1973).
[2] H. Georgi and S. L. Glashow, Phys. Rev. Lett. **32**, 438 (1974).
[3] J. Hisano, H. Murayama, and T. Yanagida, Nucl. Phys. **B402**, 46 (1993).
[4] H. Murayama and A. Pierce, Phys. Rev. D **65**, 055009 (2002).
[5] H. Nishino *et al.* (Super-Kamiokande Collaboration), Phys. Rev. Lett. **102**, 141801 (2009).
[6] H. Nishino *et al.* (Super-Kamiokande Collaboration), Phys. Rev. D **85**, 112001 (2012).
[7] K. Kobayashi *et al.* (Super-Kamiokande Collaboration), Phys. Rev. D **72**, 052007 (2005).
[8] C. Regis *et al.* (Super-Kamiokande Collaboration), Phys. Rev. D **86**, 012006 (2012).
[9] P. Nath and P. Fileviez Perez, Phys. Rep. **441**, 191 (2007).
[10] K. Abe *et al.*, arXiv:1109.3262.
[11] Y. Hara, S. Itoh, Y. Iwasaki, and T. Yoshie, Phys. Rev. D **34**, 3399 (1986).
[12] K. C. Bowler, D. Daniel, T. D. Kieu, D. G. Richards, and C. J. Scott, Nucl. Phys. **B296**, 431 (1988).
[13] M. B. Gavela, S. F. King, C. T. Sachrajda, G. Martinelli, M. L. Paciello, and B. Taglienti Nucl. Phys. **B312**, 269 (1989).
[14] S. Aoki *et al.* (JLQCD) Phys. Rev. D **62**, 014506 (2000).
[15] N. Tsutsui *et al.* (CP-PACS), Phys. Rev. D **70**, 111501 (2004).
[16] Y. Aoki, C. Dawson, J. Noaki, and A. Soni, Phys. Rev. D **75**, 014507 (2007).
[17] Y. Aoki, P. Boyle, P. Cooney, L. Del Debbio, R. Kenway, C. Maynard, A. Soni, and R. Tweedie (RBC and UKQCD), Phys. Rev. D **78**, 054505 (2008).
[18] Y. Aoki *et al.* (RBC and UKQCD), Phys. Rev. D **83**, 074508 (2011).
[19] S. Weinberg, Phys. Rev. Lett. **43**, 1566 (1979).
[20] F. Wilczek and A. Zee, Phys. Rev. Lett. **43**, 1571 (1979).
[21] L. F. Abbott and M. B. Wise, Phys. Rev. D **22**, 2208 (1980).
[22] C. Alexandrou, S. Gusken, F. Jegerlehner, K. Schilling, and R. Sommer, Nucl. Phys. **B414**, 815 (1994).
[23] M. Lin *et al.* (RBC and UKQCD), Proc. Sci., LATTICE (**2012**) 172.
[24] T. Yamazaki, Y. Aoki, T. Blum, H. Lin, M. Lin, S. Ohta, S. Sasaki, R. Tweedie, and J. Zanotti (RBC and UKQCD), Phys. Rev. Lett. **100**, 171602 (2008).
[25] T. Yamazaki, Y. Aoki, T. Blum, H. Lin, S. Ohta, S. Sasaki, R. Tweedie, and J. Zanotti, Phys. Rev. D **79**, 114505 (2009).
[26] T. Blum, T. Izubuchi, and E. Shintani, Phys. Rev. D **88**, 094503 (2013).